Journal of Applied Polymer Science

Impact of titanium and silica/titanium fumed oxide nanofillers on the elastic properties and thermal decomposition of a polyester resin

Borys Gorelov,[1] Alla Gorb,[2] Oleg Korotchenkov,[2] Andriy Nadtochiy,[2] Oleksiy Polovina,[2] Nadia Sigareva[1]

[1]Chuiko Institute of Surface Chemistry of the National Academy of Sciences of Ukraine, Kyiv 03164, Ukraine

[2]Taras Shevchenko Kyiv National University, Kyiv 03127, Ukraine

Correspondence to: A. Gorb (E-mail: g_alla@ukr.net)

ABSTRACT: The impact of nanoparticles of titanium (rutile) and silica–titanium fumed oxide (STO) on both the acoustic properties and thermal decomposition of a styrene-crosslinked unsaturated polyester resin were studied with the methods of ultrasonic probing and thermal decomposition mass spectrometry at filler loadings ranging from 0.5 to 5.0%. It was shown that the elastic modulus, Poisson's ratio, and thermal resistivity in the titanium-filled nanocomposites increased at small loadings of about 0.5%, whereas in the STO-filled nanoparticles, the decreases in the parameters at loadings of up to 1.5% was replaced by some increases at higher loadings of up to 5.0%. Distinctions in the concentration dependences of the elastic parameters and the thermal decomposition intensity for both fillers could be explained by the features of the polymer–particle interactions because of the differences in both the number of active sites located on the particle's surface and the polymer structure within interface regions. © 2015 Wiley Periodicals, Inc. J. Appl. Polym. Sci. **2015**, *132*, 42010.

KEYWORDS: composites; mechanical properties; nanoparticles; nanowires and nanocrystals; resins; thermal properties

Received 10 September 2014; accepted 18 January 2015

DOI: 10.1002/app.42010

INTRODUCTION

Both titanium and silicon dioxide nanosized particles have been widely used to extend the functional characteristics of polymer composites.[1–5] For example, the embedding of titanium dioxide (TiO_2) nanoparticles into thermosetting polymers and elastomers results in enhancements in their thermal resistance,[6–8] stiffness and toughness,[9] thermal conductivity,[10] tensile properties,[8,11] impact strength,[11] and fracture toughness.[11] It is remarkable that the aforementioned improvements manifest themselves at low filler contents ($\leq$5 wt %) and are related to the stabilization of the polymer's inner structure because of the binding of macromolecular chains to the superficial centers of the particles.[6,12–15]

The unsaturated polyester resin (UPR), which belongs to thermosetting polymers, demonstrates a good combination of mechanical and electric parameters and resistivity to chemically aggressive environments, and it is a good matrix for preparing composite materials with improved functional parameters.[16–25] In addition, because of the relatively low cost of the polyester resin, its composites are promising it's the manufacture of construction components in both domestic and industrial applications.[26]

It is known that concentration effects of inorganic oxide nanoparticles of a high surface-active site number on the physical parameters of polymer composites have an unmonotonic character. For example, the addition of a small amount of nanosized SiO_2 particles into a styrene-crosslinked polyester resin not only results in an enhancement of the composite's thermal resistance, but it is also able to either suppress[16] or stimulate[20] the emanation of styrene. All of these issues are induced with the same effect of polymer structure stabilization because of the fastening of both polyester macromolecular chains and styrene links to the superficial centers of SiO_2.

It is also known that the filling of polymers with nanoparticles of a neutral surface can result in an improvement in their performance.[27]

The physical nature of an enhancement induced with nanoparticles in the mechanical and thermal parameters of polymer nanocomposites is poorly lighted.

In this study, we dealt with the impact of the filling nanoparticles of relatively low surface-active site number on the heat-resistance and acoustic properties of polymer nanocomposites. Nanosized particles of titanium (rutile form) and silica–titanium were used as fillers in a styrene-crosslinked UPR.

The concentration-related impact of each filler on the thermal decomposition of the composites and their dynamic mechanical parameters in a field of acoustic vibrations were experimentally studied.

EXPERIMENTAL

The UPR matrix was commercially available (Polymal 1094 AWTP-1 orthophthalic polyester resin, Poland). The nanofillers were TiO_2 of the rutile form (Ukraine) with a low surface reactivity and silica–titanium fumed oxide (STO; ST-40, Ukraine). The titanium particles were characterized with average diameters of $2R_f \approx 25$ nm and a specific surface area of $S_f \approx 10$ m^2/g, whereas the STO particles had characteristic values of $2R_f \approx 40$ nm and $S_f \approx 40$ m^2/g. For both fillers, their mass concentration (C_f) in the composites were varied as follows: 0.5, 1.5, 3.0, and 5.0%.

The preparation of the nanocomposite samples of every composition was performed separately for every filler loading. The preparation procedure included the following sequence:

1. First, the hardener was added to the weighted amount of the initial resin solution in a proportion set by the product specifications, and then, the solution was mixed for 2 min.
2. Second, filler powder of a necessary amount was added to the solution obtained from the first step and mixed carefully for 10−15 min to obtain a mixture of a homogeneous consistency (both a low viscosity of the initial resin solution and a good wettableness of the filler surface assisted to obtain good homogeneity with no additional ultrasonic treatment of the mixture).
3. The mixture prepared in step 2 was poured out in forms, where it cured at a room temperature for 72 h.

It should be noted that the commercially available filler powder was annealed for 1.5 h at 350−400°C before it was used to activate its surface.

Experimental studies were carried out with the ultrasound probing technique[28] and programmable thermal desorption combined with the mass spectroscopic detection of emanating atomic species.[29]

Sound velocity measurements were performed by the phase-frequency technique in a continuous wave mode of operation.[28] The experimental setup contained a PC-controlled frequency synthesizer, which fed the input piezoelectric transducer via a power amplifier. An excited elastic wave of circular frequency (ω) propagated along the sample and was then detected with the output piezoelectric transducer. The phase shift [$\varphi(\omega)$] between the input and output electric signals was detected with a phase detector, digitized, and transferred to a computer for processing. Different pairs of transducers were used to excite longitudinal and shear waves separately. The measurements were carried out within the frequency range of 1.5−2.0 MHz, where the ultrasound vibrations suffered both negligible dispersion and high attenuation. The group delay time (T_g) and group velocity of elastic wave propagation were determined by well-known relations.[28] The longitudinal wave-phase velocity (V_L) and shear wave-phase velocity (V_S) were calculated via group velocity in the case of negligible dispersion.

The samples for the ultrasonic measurements were of a squared parallelepiped shape with lateral sides of 8−9 mm and a length (L) of 24−26 mm. Sample sizes and measuring ω were chosen to make the interference of elastic waves within the sample negligible.

To exclude an overestimation of T_g because of the propagation of the wave through both the transducers, every measurement was made with two samples of different lengths (L_1 and $L_2 = L_1/2$).

The corresponding T_g values were determined as inclination angle tangents of the correspondent lines; this approximated the experimental dependencies of φ versus ω via the least squares method. It was proven that the dependences $\varphi(\omega)$, which were measured experimentally, were so close to linear ones that the relative errors in T_g, V_L, and V_S did not exceed 0.7%.

Then, the elastic constants (C_{11} and C_{44}) were evaluated via measured values of V_L and V_S and the calculated value of the composite density (ρ_C) with the following formulas:[28]

$$C_{11} = \lambda_C + 2\mu_C = \rho_C V_L^2 \quad (1)$$

$$C_{44} = \mu_C = \rho_C V_S^2 \quad (2)$$

where λ_C and μ_C are the Lame constants.[28] As maximal variations in ρ_C for both the fillers (obtained for $C_f = 5.0\%$) were no more than 0.4%, we used calculated but not measured ρ_C values in the estimation of both C_{11} and C_{44}. The values of $\rho_C(C_f)$ were calculated with the following formula, which could be easily found from elementary considerations:

$$\rho_C = \rho_C(C_f) = \frac{\rho_m \rho_f}{\rho_m C_f + \rho_f (1 - C_f)} \quad (3)$$

where ρ_m is the density of the polymer matrix ($\rho_m = 1.2 \times 10^3$ kg/m^3)[30] and ρ_f is the density of the filling material (we used $\rho_{f1} = 4.2 \times 10^3$ kg/m^3 for TiO_2 and $\rho_{f2} = 3.26 \times 10^3$ kg/m^3 for $Si_XTi_{1-X}O_2$ calculated as the average between ρ_{f1} and 2.32×10^3 kg/m^3 of SiO_2).[31,32] Thus, the relative errors in the estimation of these elastic constants did not exceed 1.5% for C_{11}, C_{44}, and μ_C and 3.0% for λ_C.

Finally, a set of mechanical parameters, including the Young's modulus (E_C), compression modulus (M_C), and Poisson's ratio (v_C) were calculated via λ_C and μ_C with the corresponding expressions, which are valid for rod-shaped samples:[28]

$$E_C = \mu_C(3\lambda_C + 2\mu_C)/(\lambda_C + \mu_C) \quad (4)$$

$$v_C = 0.5\lambda_C/(\lambda_C + \mu_C) \quad (5)$$

$$M_C = \lambda_C + 2\mu_C/3 \quad (6)$$

The relative errors in estimations of E_C, M_C, and v_C did not exceed 1.5, 2.6, and 1%, respectively.

A content of volatile products emanated by the samples during their thermal destruction were determined with a programmable thermal desorption technique combined with mass spectroscopic detection.[29] To carry out mass spectroscopic analysis, a sample of about 10^{-3} g was inserted into a quartz–molybdenum tube pumped out to a pressure of 10^{-1} Pa. The tube was mounted into a microprocessor-controlled heater operating within the

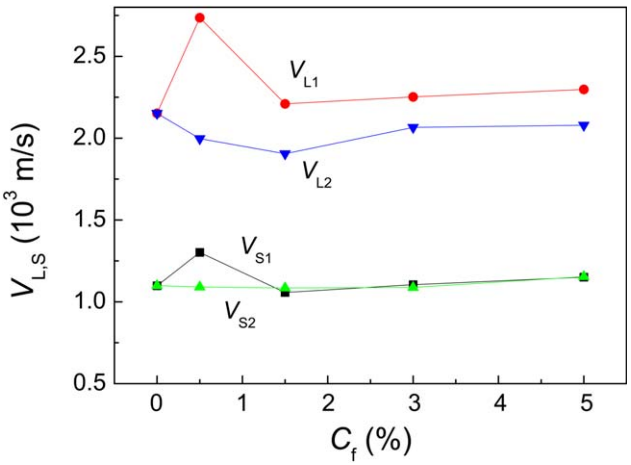

Figure 1. Concentration dependence of the V_L and V_S values measured in the UPR-based nanocomposites filled with TiO_2 (V_{L1} and V_{S1}) and STO (V_{L2} and V_{S2}) where, V_L and V_S are the ultrasound phase velocities measured in the samples by using longitudinal and shear waves, correspondently. [Color figure can be viewed in the online issue, which is available at wileyonlinelibrary.com.]

temperature range 25−900°C. The heating rate did not exceed 8°C/min. Destruction fragments were flying out the of tube and passing through a high-vacuum lock into another 20-cm-long quartz tube terminated with an input circuit of a single-pole mass analyzer (MX7304A) with a measurement range of 1−400 Da and a sensitivity of 10^{-8} g. The analyzer was tuned to detect the single-ionized species only. The sample's temperature was measured with an accuracy of ±0.05°C. The thermal decomposition mass spectra were recorded under conditions when both the shape and position of the decomposition peaks depended on neither the interface temperature nor the sample's mass. These conditions enabled us to exclude nonuniform temperature distribution within a sample and thus prevent the creation of secondary volatile products as a result of interactions among the initial molecular fragments of the polymeric chain decomposition process.

RESULTS AND DISCUSSION

Ultrasonic Probing

The concentration dependencies of both the V_L and V_S values measured in the UPR-based nanocomposites filled with TiO_2 (V_{L1} and V_{S1}, respectively) and STO (V_{L2} and V_{S2}, respectively) are shown on Figure 1. The velocities measured with unfilled resin [$V_L(C_f = 0) = 2.15 \times 10^3$ m/s and $V_S(C_f = 0) = 1.10 \times 10^3$ m/s] were both in good agreement with the ones available in the literature.[33] We observed that $V_L(C_f)$ demonstrated a nonmonotonous behavior within the interval of $C_f < 3.0\%$, where for TiO_2-filled nanocomposites, V_{L1} increased and reached its maximum at 0.5%, whereas for STO-filled nanocomposites, V_{L2} decreased. As C_f increased further, $V_{L1}(C_f)$ increased, and $V_{L1}(5.0\%) > V_L(0)$. For the STO-filled nanocomposites, $V_{L2}(C_f)$ increased in the range $3.0\% < C_f \leq 5.0\%$, but here, $V_{L2}(5.0\%) < V_L(0)$. It was remarkable that the inequality $V_{L1}(C_f) > V_{L2}(C_f)$ took place at any value of C_f.

V_{S1} and V_{S2} demonstrated different behavior at $C_f \leq 1.5\%$, where $V_{S1} > V_{S2}$. At $C_f > 1.5\%$, $V_{S1} \approx V_{S2}$, and both velocities increased slowly as C_f increased (see Figure 1).

As shown in the eqs. (1) and (2), filler-induced variations in both V_L and V_S were due to changes occurring in both ρ_C and the elastic parameters (μ_C and λ_C). Numerical estimations with eq. (3) showed that maximal increments in ρ_C occurred at $C_f = 5\%$, where $[\rho_C\ (5\%) - \rho_m]/\rho_m$ was equal to 3.3% for titanium and 3.7% for STO. Such increments could promote a drop of no more than 2% in either $V_{L1,2}$ or $V_{S1,2}$, provided that μ_C and λ_C remained unchanged. Of course, there were no reasons to expect the resin's elastic parameters to be unchanged under the filler's loading. Moreover, we could evaluate the concentration dependences of μ_C and λ_C in particulate composites with the micromechanical models available in the literature. For example, numerical calculations by the Christensen–Lo model predicted a linear increasing in both μ_C and λ_C with increasing concentration in the range $0 < C_f < 5.0\%$.[34] Namely, we found that $[\mu_{C1}(5.0\%) - \mu_0]/\mu_0 \approx 3\%$ and $[\lambda_{C1}(5.0\%) - \lambda_0]/\lambda_0 \approx 2.4\%$ for the TiO_2-filled nanocomposites and $[\mu_{C2}(5.0\%) - \mu_0]/\mu_0 \approx 4.1\%$ and $[\lambda_{C2}(5.0\%) - \lambda_0]/\lambda_0 \approx 3.3\%$ (λ_0 and μ_0 are the Lame constants of the unfilled resin) for the STO nanocomposites. With the previous estimations of ρ_C, μ_C, and λ_C taken into account, we evaluated [with eqs. (1) and (2)] the linear variations in the composite's velocities with increasing C_f in the range $0 < C_f < 5.0\%$, namely, the decreasing V_S and V_L in the TiO_2 nanocomposites $[V_{L1}(5.0\%)/V_L(0) \approx 0.995$ and $V_{S1}(5.0\%)/V_S(0) \approx 0.996]$ and their increases in the STO nanocomposites $[V_{L2}(5.0\%)/V_L(0) \approx 1.003$ and $V_{S2}(5.0\%)/V_S(0) \approx 1.005]$. The discrepancies between the calculations and the experimental data were due to the fact that the Christensen–Lo model did not take the filler–matrix interactions into account. Therefore, we concluded that nonmonotonous concentration behaviors of the phase velocities observed in both composites resulted from structural changes in the polymer network occurring in the vicinity of the nanoparticles. The structural changes could be imaged as rearrangements in the polyester chains and styrene crosslinks because of their interactions with the particles. The rearrangements were accompanied by local changes in the binding energy and, thus, revealed themselves as variations in the overall elastic parameters of the composites.

Figures 2 and 3 show the concentration behavior of the elastic parameters in the nanocomposites filled with titanium (curve 1) and STO (curve 2). Here, the average values of the elastic parameters measured for the unfilled resin were as follows: $\mu_0 = 1.4\ 5 \times 10^9$ N/m^2, $M_0 = 3.63 \times 10^9$ N/m^2, $E_0 = 3.835 \times 10^9$ N/m^2 where M_0 and E_0 are the Young's and compression modules, correspondently, of the unfilled resin, and $v_0 = 0.324$ where v_0 is the Poisson's ratio of the unfilled resin. When comparing Figure 2 with Figure 1, one can see that for both the fillers, the concentration dependencies of the shear modulus [μ_C; Figure 2(a)] were similar to those of V_S, whereas the $M_C(C_f)$ curves [Figure 2(b)] resembled the $V_L(C_f)$ ones. It is known that the M_C and μ_C modulus characterize, accordingly, short-range and long-range atomic interactions in polymers.[35] Therefore, large increments in both moduli of the TiO_2 nanocomposites observed at $C_f = 0.5\%$ compared to the unfilled resin testified to the jumplike increases in the shear and volume deformations of the composites and a weakening in the atomic interactions on the polymer–TiO_2 interfaces.

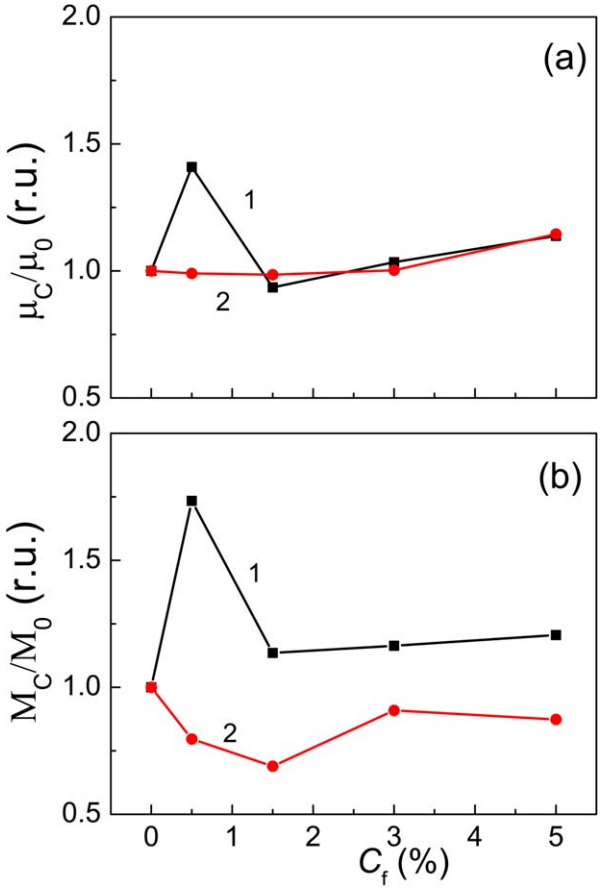

Figure 2. Normalized concentration dependence of the (a) shear (μ_C) and (b) compression (M_C) modules in the nanocomposites filled with (1) TiO_2 and (2) STO. For the unfilled resin $\mu_0 = 1.45 \times 10^9$ N/m^2, $M_0 = 3.63 \times 10^9$ N/m^2. [Color figure can be viewed in the online issue, which is available at wileyonlinelibrary.com.]

Unlike TiO_2, STO particles were added to the resin and poorly influenced the concentration-related behavior of both μ_C and the shear deformations. Unmonotonic decreasing of M_C indicated a reduction in the composite volume deformation under dynamic loading and an enhancement of the interatomic interactions on the polymer–STO interfaces.

Comparing Figure 3 with Figure 2, one can see that the concentration dependences of E_C and v_C were similar to those of $\mu_C(C_f)$ and $M_C(C_f)$, respectively.

A large increment (~50%) in E_C of the TiO_2-filled nanocomposites observed in the vicinity of $C_f = 0.5\%$ testified to a reduction in the composite's deformation under longitudinal dynamic loading caused by an acoustic wave. Also, a yet greater increment (~75%) in v_C at $C_f = 0.5\%$ evidenced the fact that shear deformation exceeded the longitudinal deformation in the TiO_2 nanocomposites.

A weak and unmonotonous lowering of E_C in the STO-filled nanocomposites observed in the concentration range of $0 < C_f \leq 3\%$ [see Figure 3(a)] specified the insignificant unmonotonous increase in the nanocomposite's deformation under its longitudinal dynamic loading. Also, in the STO nanocomposites, a behavior of v_C within the same concentration range [see Figure 3(b)] showed that the longitudinal deformation exceeded the transversal one, and such behavior was opposite to that which was observed in the TiO_2 nanocomposites.

Thus, ultrasonic probing showed that in the range of small nanoparticle loadings, the nanocomposites of the styrene-crosslinked polyester resin filled with either titanium or STO exhibited different characteristics of interatomic interactions in the vicinity of the nanoparticles and the opposite behavior of longitudinal and transversal deformations in the ultrasonic stress field.

Thermal Decomposition Mass Spectroscopy

The mass spectrum of the positively charged volatile products of the thermally induced decomposition of the resin obtained at the temperature corresponding to the maximum intensity of the product's lines is presented in Figure 4. The assignment of the m/z [m is the atomic mass and z is a degree of ionization of the volatile products ($z = +1$ in our experiments)] decomposition fragments shown in Figure 4 was performed because of the structural formula of the polyester resin, which consisted of the polyester chains [$CH_2OOC{-}(CH)_2{-}COOCH_2{-}CH_2O{-}$] and the styrene crosslinks ($-H_2C{-}HC{-}C_6H_5$).[36] Lines appearing in m/z

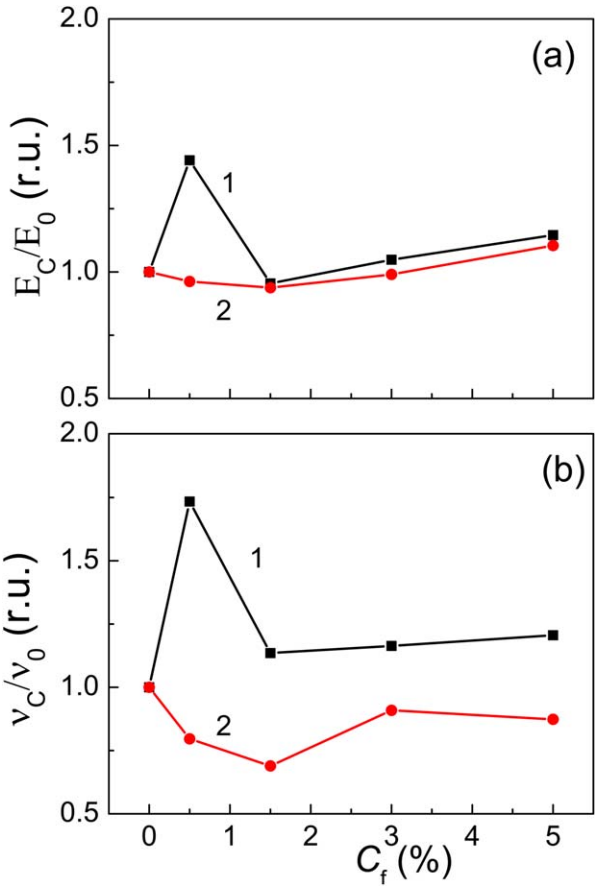

Figure 3. Normalized concentration dependence of the (a) Young's modulus (E_C) and (b) Poisson's ratio (v_C) in the nanocomposites filled with (1) TiO_2 and (2) STO. For the unfilled resin $v_0 = 0.324$ and $E_0 = 3.835 \times 10^9$ N/m^2. [Color figure can be viewed in the online issue, which is available at wileyonlinelibrary.com.]

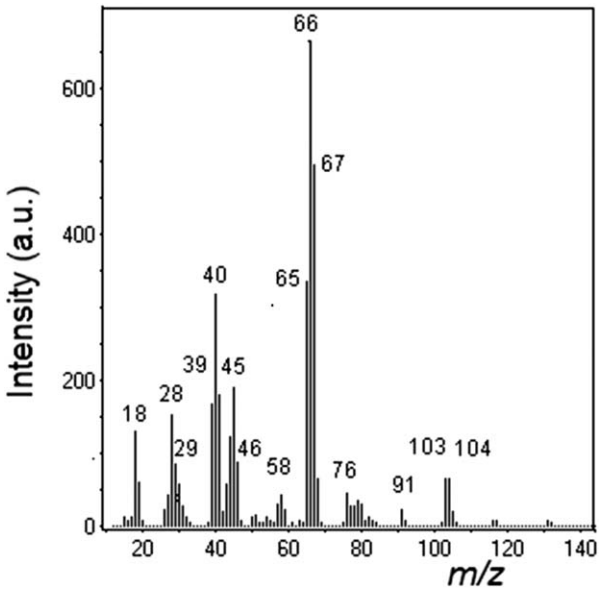

Figure 4. Mass spectra of the thermal decomposition volatile products for the unfilled polyester resin measured at 280°C.

intervals of $27 \leq m/z \leq 31$ and $44 \leq m/z \leq 59$ were assigned to the fragments of the thermal decomposition of the polyester chains, such as $-CHCH_2$ (27), CO (28), OCH_2 (30), COO (44), OCH_2CH_2 (44), OOCH (45), $OOCH_2$ (46), COOCH (57), and $COOCH_2$ (58). The lines appearing in m/z intervals of $39 \leq m/z \leq 41$, $65 \leq m/z \leq 67$, and $76 \leq m/z \leq 105$ were assigned to the fragments of the thermal decomposition of the styrene crosslinks, such as $(CH)_3$ (39), $CHCH_2CH$ (40), $CHCHCH_2CHCH$ (66), C_6H_4 (76), C_6H_5 (77), C_6H_6 (78), $C_6H_5CH_2$ (91), $C_6H_5CHCH_2$ (104), and $C_6H_5CHCH_3$ (105).

Under the thermal decomposition of the unfilled resin, the polyester chain fragment of $m/z = 44$ (COO or OCH_2CH_2) released in the temperature interval 65−430°C [Figure 5(a,b), curve 1]. The curve exhibited two peaks centered at thermal decomposition peak positions (T_m's) of about 195 and 395°C. The appearance of the thermally stimulated decomposition at temperatures of $T \leq 250$°C indicated the presence in the structure of unlinked polyester chain segments containing a complex ether.[37] The second peak ($T_m \sim 395$) was related to the decomposition of the bulk of the polymer.[37]

To discriminate correctly between COO and OCH_2CH_2 in the $m/z = 44$ decomposition products, we compared the thermal decomposition curve of $m/z = 44$ with the one of $m/z = 45$. Both curves appeared to be very close to each other. Therefore, we supposed that the $m/z = 44$ product was mainly due to the COO moiety.

Filling the resin with nanosized particles of titanium and STO rendered a different influence on the thermal decomposition of the nanocomposites. The addition of TiO_2 particles into the resin changed the dynamics of the thermal decomposition process. The thermal decomposition weakened at a small filler concentration of 0.5%, and the yield of volatile products decreased. The thermal decomposition curve contained the two peaks positioned at $T_m \approx 155$ and 350°C [Figure 5(a), curve 2]. Increasing C_f above 0.5% resulted in an enhancement of the chain's thermal decomposition within the temperature range 250−450°C and in an increase in the amount of volatile fragments. The temperature positions of both peaks underwent no changes (Figure 5, curves 2 and 3).

Filling the resin with STO nanoparticles enhanced the thermal decomposition of the nanocomposites with increasing filler content, which caused the volatile product yield to grow. However, the thermal stability of the nanocomposites at $C_f \leq 1.5\%$ changed unmonotonously at temperatures below 215°C, where unbound or unlinked segments of polyester macromolecular

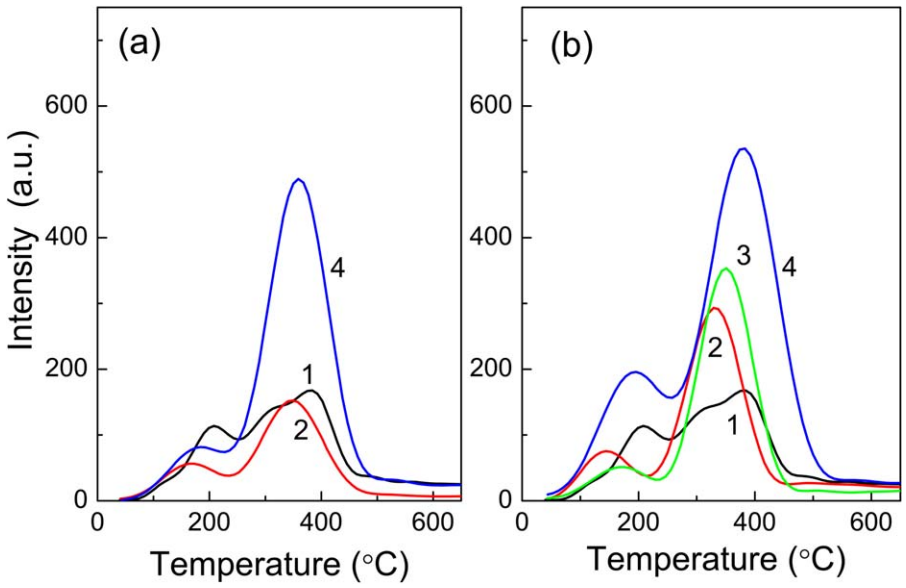

Figure 5. Thermal decomposition curves for the polyester chain fragments at $m/z = 44$ (COO, $OCHCH_2$) for (1) the unfilled resin and its nanocomposites filled with (a) TiO_2 at $C_f =$ (2) 0.5 and (4) 3.0% and (b) STO at $C_f =$ (2) 0.5, (3) 1.5, and (4) 3.0%. [Color figure can be viewed in the online issue, which is available at wileyonlinelibrary.com.]

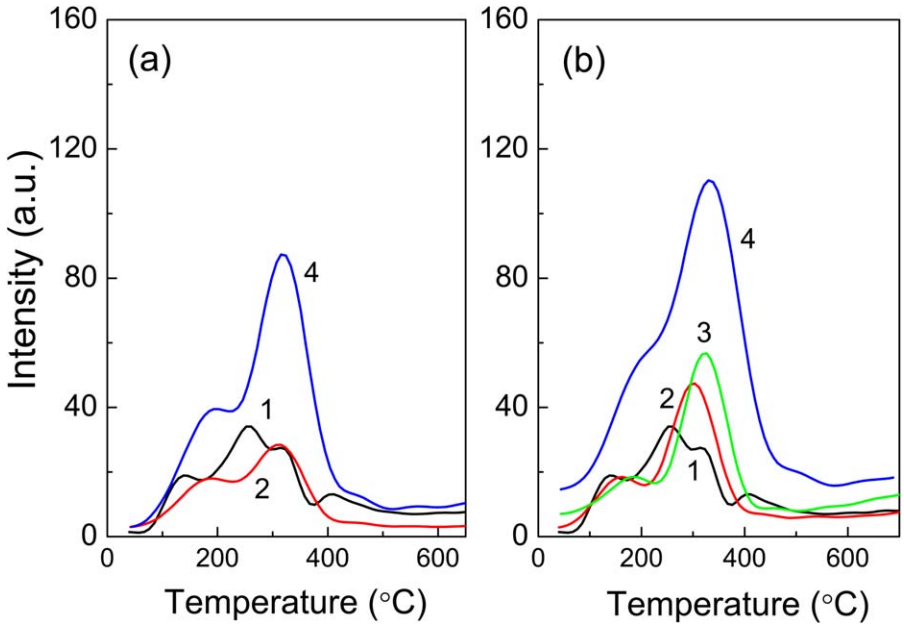

Figure 6. Thermal decomposition curves for the polyester chain fragments at $m/z = 57$ (COOCH) for (1) the unfilled resin and its nanocomposites filled with (a) TiO_2 at $C_f = (2)$ 0.5 and (4) 3.0% and (b) STO at $C_f = (2)$ 0.5, (3) 1.5, and (4) 3.0%. [Color figure can be viewed in the online issue, which is available at wileyonlinelibrary.com.]

chains were destroyed. The thermal stability of the nanocomposites increased with increasing C_f at $C_f < 1.5\%$ because the yield of volatile products decreased. When C_f was increased up to 3%, the volatile product yield continued to grow, and T_m rose to 196°C; that is, the thermal stability decreased. Unmonotonous changes in the thermal stability observed at temperatures of $T \leq 215$°C indicated an unmonotonous reduction in the number of unbound polyester chain segments [see Figure 5(b)].

The bulk of the polymer matrix in the STO-filled nanocomposites decomposed in the temperature range 220−420°C. As C_f increased to 3%, the yield of $m/z = 44$ products (COO and $OCHCH_2$) increased, the peak intensity of the corresponding thermal decomposition band grew, and the position of T_m was displaced toward high temperatures to 394°C. Also, the decomposition band broadened toward high temperatures to 515°C [Figure 5(b)]. Both the increase in T_m and the broadening of the band was assigned to an increase in the decomposition activation energy of the corresponding fragments as a result of changes in the polymer structure conformation due to the fastening of the fragments on the active surface sites of the nanoparticles.

For both fillers, their concentration effects on the thermal decomposition of the longer polyester chain fragment of COOCH ($m/z = 57$) were similar to those of the $m/z = 44$ fragments (COO and $OCHCH_3$). In the TiO_2 nanocomposites at $C_f = 0.5\%$, the thermal stability grew slightly because a decrease in the fragment's yield was scarcely noticeable. As C_f increased to 3.0%, the thermal decomposition of the nanocomposite increased; that is, the yield of the fragment increased over the entire temperature range [see Figure 6(a)].

In the STO-filled nanocomposites, when $C_f \leq 1.5\%$, the intensity of thermal decomposition practically did not change at $T \leq 200$°C. However, at higher temperatures, the decomposition was enhanced, and T_m was displaced toward high temperatures. When C_f was increased to 3.0%, the decomposition was enhanced over the entire range, T_m was displaced toward 350°C, and the decomposition band broadened toward high temperatures to 560°C [see Figure 6(b)].

The thermal decomposition curves related to the fragments of styrene molecules, such as C_6H_5 ($m/z = 77$) and $C_6H_5CHCH_2$ ($m/z = 104$), reflected the filler's impact on the styrene crosslink destruction (see Figure 7). The addition of titanium nanoparticles to the resin in an amount of $C_f \leq 0.5\%$ caused the yield of styrene-related decomposition fragments to decrease, and thus, this enhanced the thermal stability of the nanocomposites over the entire temperature interval [see Figure 7(a,c), curve 2]. Such a decrease in the yield of the styrene-related fragments testified that TiO_2 nanoparticles resulted in a simultaneous lowering of the number of styrene fragments unbound with polyester chains, which decomposed at $T \leq 220$°C, and also in the strengthening of the styrene crosslinks, which underwent thermal decomposition within the temperature range 290–440°C.

Increasing the TiO_2 loading up to $C_f = 3.0\%$ enhanced the decomposition of styrene crosslinks, and as a consequence, the yield of styrene decomposition fragments increased over the entire temperature range. Also, the decomposition band centered at $T_m \approx 370$°C broadened toward high temperatures to 480°C [Figure 7(a,c) the curve 3]. Such a high-temperature broadening of the thermal decomposition band showed that the styrene crosslinks weakened the number of both unbound C_6H_5 and $C_6H_5CHCH_2$ fragments, and the number of fragments fastened to the active surface sites of the particles increased.

The filling of the resin with STO nanoparticles at $C_f \leq 1.5\%$ had no influence on the thermal decomposition of unbound styrene

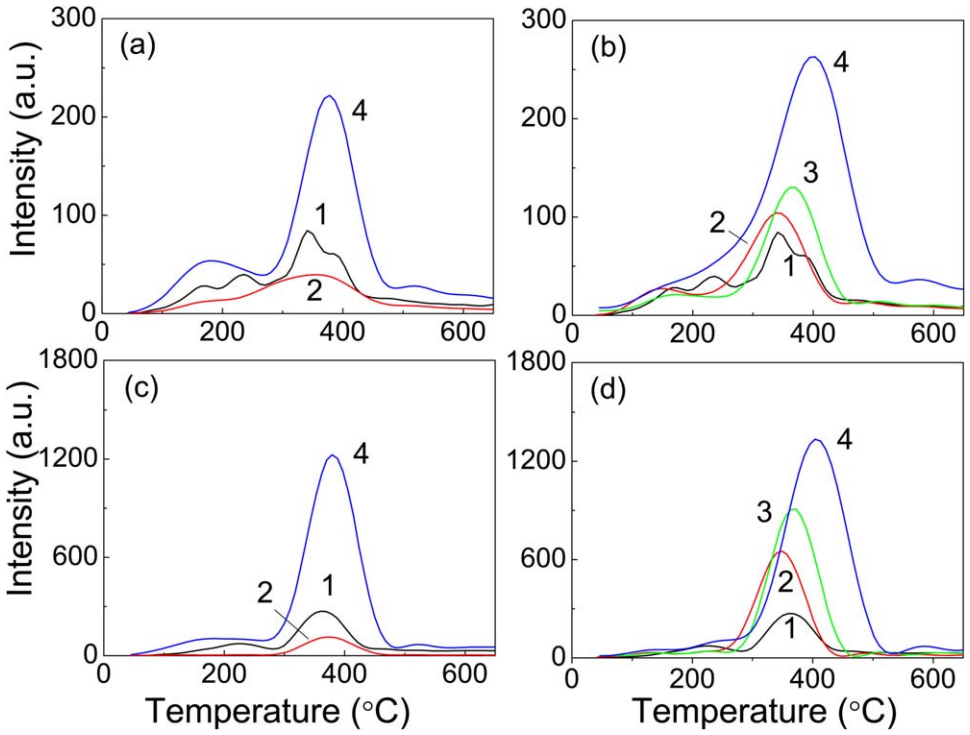

Figure 7. Thermal decomposition curves for the styrene crosslink fragments at m/z = (a,b) 77 (C_6H_5) and (c,d) 104 ($C_6H_5CHCH_2$) for (1) the unfilled resin and its nanocomposites filled with (a,c) TiO_2 at C_f = (2) 0.5 and (4) 3.0% and (b,d) STO at C_f = (2) 0.5, (3) 1.5, and (4) 3.0%. [Color figure can be viewed in the online issue, which is available at wileyonlinelibrary.com.]

fragments (C_6H_5 and $C_6H_5CHCH_2$) in the range of $T \leq 220-230$°C. As C_f increased, the following changes were visible in the thermal decomposition curves shown in Figure 7. The yield of both fragments grew in the temperature range 270−450°C; this indicated an enhancement of the thermal decomposition of the styrene crosslinks, both the decomposition bands broadened toward high temperatures to 530°C, and the T_m positions of the bands were shifted from 330 to 400−430°C [see Figure 7(b,d), curves 2–4]. In addition, at C_f = 3.0%, a weak line centered at about 585°C emerged on every curve within the temperature range 550−620°C. Such an evolution of the decomposition curves testified that the STO nanoparticles exerted little influence on the number of unbounded styrene molecules and their decomposition; however, the particles promoted the thermal decomposition of the styrene crosslinks. Moreover, at C_f = 3.0%, the fragments of styrene molecules fastened onto the particles via their active surface sites. This was the reason that resulted in the appearance of the aforementioned high-temperature decomposition bands and an increase in the decomposition activation energy for the styrene-related fragments.

It should be noted that the STO particles had a far greater number of chemically active sites on their surface than the titanium (rutile) ones. This was shown with IR spectroscopy measurements. Figure 8 compares the IR absorption spectra of various filling nanoparticles: silica (A-300, $S_f \approx 280$ m^2/g, curve 1), STO ($S_f \approx 40$ m^2/g, curve 2), TiO_2 (anatase, $S_f \approx 95$ m^2/g, curve 3), and TiO_2 (rutile, $S_f \approx 10$ m^2/g, curve 4). The spectrum of STO (curve 2) contained the bands of free OH groups (3750 cm^{-1}) and the absorption centers of [Ti—O(H)—Ti; 1454 cm^{-1}]. Such centers are also present in the IR spectra of both silica and anatase. Neither such centers nor other ones were present on the surface of the rutile TiO_2. Thus, it was less active catalytically.

In addition, the IR spectra of the STO particles were analogous to the spectrum of anatase. This specified that the titanium domains on the surface of STO had the mineral form of anatase. The same conclusion was drawn earlier.[38]

Thus, filling the styrene-crosslinked polyester resin with titanium nanoparticles with a weak surface reactivity exerted a nonmonotonous and dissimilar influence on the thermal decomposition of the polyester macromolecular chains and the styrene crosslinks among the chains. At a small content of TiO_2 particles ($C_f \leq 0.5\%$), the thermal decomposition of the nanocomposites weakened; that is, its thermal resistivity increased. As C_f increased, the thermal decomposition became stronger. On the other hand, a binding of the styrene molecules to the surface of the particles took place; this caused a broadening of the decomposition bands toward high temperatures.

The increase in the thermal resistivity of the TiO_2-filled nanocomposites observed at the small particle content (C_f = 0.5%) testified to the stabilization of the polymer structure. Also, decreases in the number of unlinked polyester chain segments and styrene crosslink fragments took place in the TiO_2-filled nanocomposites at C_f = 0.5%, and the latter was more expressed than the former [Figure 7(c)]. Both effects indicated a toughening of the resin molecular structure by tightly bound polymer layers surrounding the TiO_2 nanoparticles. Such

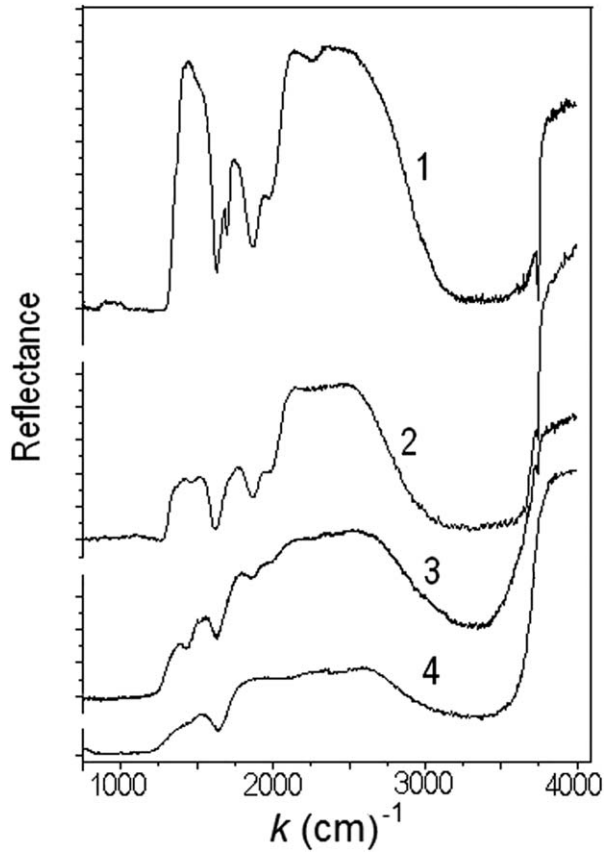

Figure 8. IR reflection spectra of filling nanoparticles: (1) silica (A-300, $S_f \approx 280$ m^2/g), (2) STO ($S_f \approx 40$ m^2/g), (3) TiO_2 (anatase, $S_f \approx 95$ m^2/g), and (4) TiO_2 (rutile, $S_f \approx 10$ m^2/g). k is the wave number of the IR-light.

structural changes were accompanied with increases in both the longitudinal and transversal acoustic wave-phase velocities (Figure 1) because of large increments in the elastic moduli, namely M_C, μ_C, and E_C [Figures 2 and 3(a)]. Moreover, an increase in v_C reflected asymmetric changes occurring in the stiffness of the polyester chains and the styrene crosslinks [Figure 3(b)].

It is known that both the stabilization and toughening of a polymeric structure is due to the binding of polymeric macromolecular chains on the surface-active sites of the nanoparticles.[39] However, enhancements in the thermal resistivity and mechanical parameters of the TiO_2-filled nanocomposites could not be explained by the stabilization of the resin structure because its macromolecular (polyester) chains did not fasten onto the TiO_2 particles because of the rather small number of surface-active sites. At the same time, the behavior of both the thermal resistivity and mechanical parameters gave evidence about the formation of stiffened areas in the nanocomposite's molecular structure.

Numerous experimental studies[40–45] and theoretical calculations[46–50] have shown that polymer–particle interfacial interactions result in the appearance of so-called interphase regions (IPRs), which surround the nanoparticles embedded in the polymer matrix. The polymer structure in such IPRs is different from those in regions remote from the nanoparticle's surface. Several models were proposed early to give qualitative descriptions for the IPR structure.[51–53] These models predict that the nanolayer closest to the nanoparticle is bound tightly to the surface; this results in the polymer chains being highly immobile. Theoretical calculations have confirmed that a particle–polymer interaction causes local increase in ρ_m near the nanosized particle.[46] The second (outer) nanolayer remote from the nanoparticle's surface is more thick and consists of loosely bound polymer chains.[54,55]

For example, in nanocomposites of polydimethylsiloxane filled with titanium nanoparticles (20−40 nm in diameter), the formation of IPRs has been suggested to result from strong hydrogen bonding between the polymer chains and hydroxyl groups present on the surface of the nanoparticles, and the thickness of the regions was estimated to 3–5 nm.[44,45] Moreover, the rearrangement of the polymer structure in the vicinity of the nanoparticles is accompanied by the formation of the electric double layer because of the difference in the dielectric permittivity between the filler and polymer.[56,57] An interaction between the surface OH groups of the rutile particles with the atoms of the surrounding electric layer seems to causes an additional adhesive force, which promotes a toughening of molecular structure of the resin near the particles. A rearrangement of the resin molecular structure reveals itself at a low filler content as reduction of the number of unbound polyester and styrene chains and a hardening of the nanocomposite. When concentration of TiO_2 particles was increased, the rearrangement of the resin structure became difficult.

The polycondensation of the polyester resin nanocomposites developed by the evolution of heterogeneous embryos with a hard polymeric phase on the surface of the nanoparticles.[58] In other words, the nanoparticles could really act as nucleating agents. However, the resulting nanocomposite was a two-phase system.

Thus, in the concentration range of TiO_2 particles of $0.5 < C_f \leq 1.5\%$, the numbers of unlinked polyester chain segments and styrene crosslink fragments increased, the contribution of loosely bound layers dominated, and the overall stiffness of the polymer network decreased. So, the process exhibited itself as decreasing both longitudinal and transversal acoustic wave-phase velocities, elastic modulus, and v_C. All of the values approached those of the unfilled resin (Figures 2 and 3).

When C_f was increased further (up to 5.0%), increasing numbers of unlinked polyester chain segments and styrene crosslink fragments were accompanied by styrene crosslinks bounded to TiO_2 particles via hydrogen and donor–acceptor bonds. Thus, small increments in acoustic parameters were assigned to an increase of ρ_C and to a partial increase of styrene crosslinks (Figures 1−3). The thermal decomposition enhancement of both the polyester chains and thermal styrene crosslinks indicated a decrease in the composite's thermal stability, and this could be explained by the increase in the number of both unbound polyester segments and styrene crosslinks and by decreases in the activation energies of the fragments of macromolecular chains (Figure 7).

The distinctions observed in the concentration behavior of the nanocomposite's elastic modulus for the different fillers could be explained by the differences in their size, intrinsic properties, and number of surface-active sites; these had an impact on both the extent and properties of the IPRs. First, the surface of the STO particles had a far greater number of surface-active sites than the surface of titanium, and thus, interactions between the particles and the polyester chains and the styrene crosslinks were stronger in the STO nanocomposites.[38] It was, therefore, possible to expect that the IPRs forming around the nanoparticles were thicker in the STO nanocomposites. Second, because the STO nanoparticles were bigger in dimension and had less density than the TiO_2 nanoparticles, the former provided a higher volume concentration in the composite at identical mass concentrations. Consequently, in the STO nanocomposites, the relative portion of IPRs was higher, and both processes occurred within the IPRs; namely, the decomposition and fastening of the polymer moieties) were more pronounced than for the TiO_2 nanocomposites. On the whole, competition between the two processes determined the concentration behavior of the elastic parameters in both nanocomposites.

The rebuilding of the resin's molecular structure caused by STO nanoparticles at $C_f \leq 1.5\%$ manifested itself as an increase in the number of unlinked polyester chain segments (Figures 5 and 6); this was accompanied by a slight change in the number of the styrene crosslinks (Figure 7). Such an asymmetrical impact of the filler on the molecular structure of the resin resulted in a reduction of V_L, whereas the transversal wave velocity remained unchanged (Figure 1). This indicated decreases in both M_C and μ_C. A decrease in V_L was observed previously in nanosilica-filled polyester resin composites, where the polyester chains were fastened to the active surface sites of the nanoparticles.[20]

Thus, an increase in the elastic parameters observed in the TiO_2 nanocomposites at $C_f \leq 0.5\%$ was assigned to the hydrogen bonds and electrostatic coupling of polar polymer moieties to the surface of the nanoparticles, whereas their decrease in the STO nanocomposites at $C_f \leq 1.5\%$ was due to the decomposition of the styrene crosslinks between the polyester chains and an increase in the portion of areas of a reduced stiffness, which contained loosely bound polyester chains.

As C_f increased from 1.5 to 5.0%, the thermal decomposition of the STO nanocomposites became stronger within the temperature region 220−420°C, and the fastening of polyester chains on the active surface sites of the particles dominated over the decomposition of the styrene crosslinks. The decomposition curves exhibited a broadening of its principal bands toward higher temperatures, and a new decomposition band of a weak intensity appeared on the curves at $T \geq 550$°C. The elastic modulus increased slowly.

CONCLUSIONS

For the STO nanocomposites, the elastic parameters decreased at $C_f \leq 1.5\%$ and reached their minimal values at $C_f = 1.5\%$; they increased slowly at $1.5\% < C_f \leq 5.0\%$. For the TiO_2 nanocomposites, the elastic parameters were maximal at $C_f = 0.5\%$; they reached their minimal values at $C_f = 1.5\%$ and then increased with increasing C_f to 5.0%.

For the STO nanocomposites, the thermal decomposition of both the polyester macromolecular chains and styrene crosslinks increased with increasing filler's concentration, whereas with the TiO_2 filler, it weakened at small filler loadings ($C_f = 0.5\%$) and increased with increasing C_f.

A correlation took place between the concentration behavior of the composite's elastic modulus and its thermal decomposition. A binding of the polymer chains to the oxides nanoparticles resulted in an increase in the thermal resistivity of the nanocomposites and an increase in the elastic modulus. The breaking of the styrene crosslinks was accompanied by an enhancement in the thermal decomposition and a decrease in the modulus. For the STO-filled nanocomposites, binding mainly caused the chemical bonds of the chain moieties to occur on active surface sites of the particles. For the titanium-filled nanocomposites, the polymer–particle interaction was mainly of an adhesive character.

TiO_2 filler of a small number of surface active sites was able to change the elastic and thermal properties of the polyester resin to the same degree as STO. The thermal decomposition of both the polyester macromolecular chains and styrene crosslinks was weakened at small filler loadings ($C_f = 0.5\%$) and increased with increasing C_f.

The distinctions observed in the concentration behavior of the elastic and thermal decomposition properties of the polyester resin nanocomposites filled with various oxides were due to differences in both the number of active sites located on the particle's surface and the polymer structure within the interface regions.

REFERENCES

1. Hussain, F.; Hojjati, M.; Okamoto, M.; Gorga, R. E. *J. Compos. Mater.* **2006**, *40*, 1511.
2. Yiu-Wing, M.; Zhong-Zhen, Y. Polymer Nanocomposites; Woodhead: Cambridge, United Kingdom, **2006**.
3. Mikitaev, A. K.; Kozlov, G. V.; Zaikov, G. E. Polymer Nanocomposites: Variety of Structural Forms and Applications; Nova Science: New York, **2008**.
4. Camargo, P. K. C.; Satyanarayana, K. G.; Wypych, F. *Mater. Res.* **2009**, *12*, 1.
5. Hanemann, T.; Szabo, D. V. *Materials* **2010**, *3*, 3468.
6. Džunuzović, E. S.; Džunuzović, J. V.; Radoman, T. S.; Marinović-Cincović, M. T.; Nikolić, L. B.; Jeremić, K. B.; Nedeljković, J. M. *Polym. Compos.* **2013**, *34*, 399.
7. Chatterjee, A. *J. Appl. Polym. Sci.* **2010**, *116*, 3396.
8. Chatterjee, A. *J. Appl. Polym. Sci.* **2010**, *118*, 2890.
9. Carballeira, P.; Haupert, F. *Polym. Compos.* **2010**, *31*, 1241.
10. Saritha, A.; Joseph, K.; Boudenne, A.; Thomas, S. *Polym. Compos.* **2011**, *32*, 1681.

11. Jyotishkumar, P.; Pionteck, J.; Moldenaers, P.; Thomas, S. *J. Appl. Polym. Sci.* **2013**, *127*, 3159.
12. Khodaparast, P.; Ounaies, Z. *IEEE Trans. Dielectr. Electr. Insul.* **2013**, *20*,166.
13. Lou, Y.; Liu, M.; Miao, X.; Zhang, L.; Wang, X. *Polym. Compos.* **2010**, *31*, 1184.
14. Ramesh, V.; Panda, B. P.; Mohanty, S.; Nayak, S. K. *Polym. Compos.* **2012**, *33*, 2177.
15. Wang, G.; Chen, G.; Wei, Z.; Yu, T.; Liu, L.; Wang, P.; Chang, Y.; Qi, M. *J. Appl. Polym. Sci.* **2012**, *125*, 3871.
16. Gorelov, B. M. *Chem. Phys. Technol. Surf.* **2011**, *2*, 201.
17. Gorelov, B. M.; Polovina, O. I.; Gorb, A. M.; Czapla, Z.; Dacko, S. *Funct. Mater.* **2012**, *19*, 493.
18. Gorelov, B. M.; Polovina, O. I.; Gorb, A. M.; Dacko, S.; Kostrzewa, M.; Ingram, A. *J. Appl. Phys.* **2012**, *112*, 094321/1.
19. Xu, Y.; Li, M.; Guo, Y.; Lu, F. *J. Mater. Sci. Technol.* **2003**, *19*, 578.
20. Gornicka, B.; Prociow, E. *Acta Phys. Polym. A* **2009**, *115*, 842.
21. Nehete, K.; Shara, R. A.; Chaudhari, L.; Bhattacharya, S.; Singal, V.; D'Melo, D. *IEEE Trans. Dielectr. Electr. Insul.* **2012**, *19*, 373.
22. Triki, A.; Guicha, M.; Hassen, M. B.; Arous, M.; Fakhfakh, Z. J. *Mater. Sci.* **2011**, *46*, 3698.
23. Monti, M.; Natali, M.; Petrucci, R.; Kenny, J. M.; Torre, L. *Polym. Compos.* **2011**, *32*, 766.
24. Poorabdollah, M.; Beheshty, M. H.; Vafayan, M. *Polym. Compos.* **2011**, *32*, 1265.
25. Hassan, T. A.; Rangari, V. K.; Jeelani, S. *J. Appl. Polym. Sci.* **2013**, *130*, 1442.
26. Pascault, J. P.; Sautereau, H.; Verdu, J.; Williams, R. Thermosetting Polymers; Marce1 Dekker: New York, **2002**.
27. Hussain, A.; Hojjati, M.; Okamoto, M.; Gorga, R. E. *J. Compos. Mater.* **2006**, *40*, 1511.
28. Royer, D.; Dieulesaint, E. Elastic Waves in Solids I: Free and Guided Propagation; Springer: New York, **2000**.
29. Pokrovsky, V. A. *J. Therm. Anal. Calorim.* **2000**, *62*, 407.
30. Grayson, M.; Eckroth, D. Encyclopedia of Chemical Technology, 3rd ed.; Wiley: New York, **1982**; p 575.
31. Ahrens, T. J. Mineral Physics and Crystallography: A Handbook of Physical Constants; American Geophysical Union: Washington, DC, **1995**.
32. Harris, M. In The RF and Microwave Handbook; Golio, M., Ed.; CRC: Boca Raton, FL, **2001**, p 9.
33. Wrobel, G. J. *Achievements Mater. Manuf. Eng.* **2007**, *20*, 295.
34. Christensen, R. M. *J. Mech. Phys. Solids* **1979**, *27*, 315.
35. Novikov, V. U.; Kozlov, G. B. *Russ. Chem. Rev.* **2000**, *69*, 347.
36. Boeing, H. V. Unsaturated Polyesters: Structure and Properties; Elsevier: Amsterdam, **1964**.
37. Pielchowski, K.; Njuguna, J. Thermal Degradation of Polymeric Materials; Rapra Technology: Shawbury, United Kingdom, **2005**.
38. Gun'ko, V. M.; Blitz, J. P.; Gude, K.; Zarko, V. I.; Goncharuk, E. V.; Nychiporuk, Y. M.; Leboda, R.; Skubiszewska-Zięba, J.; Osovskii, V. D.; Ptushinskii, Y. G.; Mishchuk, O. A.; Pakhovchishin, S. V.; Gorbik, P. P. *J. Colloid Interface Sci.* **2007**, *314*, 119.
39. Grassie, N.; Scott, G. Polymer Degradation and Stabilization; Cambridge University Press: Cambridge, United Kingdom, **1988**.
40. Chen, L.; Zheng, K.; Tian, X.; Hu, K.; Wang, R.; Liu, C.; Li, Y.; Cui, P. *Macromolecules* **2010**, *43*, 1076.
41. Harton, S. E.; Kumar, S. K.; Yang, H.; Koga, T.; Hicks, K.; Lee, HK.; Mijovic, J.; Liu, M.; Vallery, R. S.; Gidley, D. W. *Macromolecules* **2010**, *43*, 3415.
42. Picu, R. C.; Rakshit, A. *J. Chem. Phys.* **2007**, *126*, 144909.
43. Termonia, Y. *J. Polym. Sci. Part B: Polym. Phys.* **2010**, *48*, 687.
44. Klonos, P.; Panagopoulou, A.; Bokobza, L.; Kyritsis, A.; Peoglos, V.; Pissis, P. *Polymer* **2010**, *51*, 5490.
45. Klonos, P.; Pandis, C.; Kripotou, S.; Kyritsis, A.; Pissis, P. *IEEE Trans. Dielectr. Electr. Insul.* **2012**, *19*, 1283.
46. Odegard, G. M.; Clancy, T. C.; Gates, T. S. *Polymer* **2005**, *46*, 553.
47. Papakonstantopoulos, G. J.; Doxastakis, M.; Nealey, P. F.; Barrat, J.-L.; de Pablo, J. *J. Phys. Rev. E* **2007**, *75*, 031803.
48. Ndoro, T. V. M.; Voyiatzis, E.; Ghanbari, A.; Theodorou, D. N.; Böhm, M. C.; Müller-Plathe, F. *Macromolecules* **2011**, *44*, 2316.
49. Ndoro, T. V. M.; Böhm, M. C.; Müller-Plathe, F. *Macromolecules* **2012**, *45*,171.
50. Müller-Plathe, F.; Ndoro, T. V. M.; Leroy, F.; Rahimi, M.; Böhm, M. C.; Müller-Plathe, F. *Macromolecules* **2012**, *45*, 572.
51. Tsagaropoulos, G.; Eisenberg, A. *Macromolecules* **1995**, *28*, 6067.
52. Zhang, H.; Hassanali, A. A.; Shin, Y. K.; Knight, C.; Singer, S. J. *J. Chem. Phys.* **2011**, *134*, 024705.
53. Tanaka, T.; Kozako, M.; Fuse, N.; Ohki, Y. *IEEE Trans. Dielectr. Electr. Insul.* **2005**, *12*, 669.
54. Danikas, M. G. *J. Electr. Eng.* **2010**, *61*, 241.
55. Pitsa, D.; Danikas, M. G. *NANO Brief Rep. Rev.* **2011**, *6*, 497.
56. Lewis, T. J. *IEEE Trans. Dielectr. Electr. Insul.* **2004**, *11*, 739.
57. Lewis, T. J. Proceedings of 9th IEEE International Conference on Solid Dielectrics; IEEE: New York, **2007**; p 11.
58. Piorkowska, E. In Handbook of Polymer Crystallization; Piorkowska, E., Rutledge, G. C., Eds.; Wiley-VCH: Weinheim, **2013**; Chapter 13, p 379.